Journal of Catalysis 408 (2022) 388–400

Contents lists available at ScienceDirect

Journal of Catalysis

journal homepage: www.elsevier.com/locate/jcat

Evolution of the optimal catalytic systems for the oxidative dehydrogenation of ethane: The role of adsorption in the catalytic performance

Agustín de Arriba [a], Benjamin Solsona [b], Ana M. Dejoz [b], Patricia Concepción [a], Narcís Homs [c,d], Pilar Ramírez de la Piscina [c], José M. López Nieto [a,*]

[a] Instituto de Tecnología Química, Universitat Politécnica de València-Consejo Superior de Investigaciones Científicas (UPV-CSIC), Av. Naranjos s/n, 46022 Valencia, Spain
[b] Departament d'Enginyeria Química, Universitat de València, C/Dr. Moliner 50, 46100 Burjassot, Valencia, Spain
[c] Departament de Química Inorgànica i Orgànica, Secció de Química Inorgànica & Institut de Nanociència i Nanotecnologia (IN2UB), Universitat de Barcelona, Martí i Franquès 1, 08028 Barcelona, Spain
[d] Catalonia Institute for Energy Research (IREC), Jardins de les Dones de Negre 1, 08930 Barcelona, Spain

ARTICLE INFO

Article history:
Received 25 February 2021
Revised 26 May 2021
Accepted 14 July 2021
Available online 21 July 2021

Keywords:
ODH ethane
Ethylene
FT-IR adsorbed ethylene
Microcalorimetry
MoVTeNb
Promoted NiO

ABSTRACT

Three samples that correspond to the evolution of optimal catalytic systems for the oxidative dehydrogenation of ethane have been synthesized and compared in terms of catalytic behavior and adsorption properties: (i) vanadium oxide supported on alumina, (ii) Sn-promoted NiO, and (iii) multicomponent MoVTeNbO with the M1 structure. The main difference in catalytic performance lies in the extent of the overoxidation of the ethylene formed, following the order VOx/Al_2O_3 > NiSnOx > MoVTeNb-M1. Accordingly, the selectivity to ethylene at medium and high ethane conversion follows the order MoVTeNb-M1 > NiSnOx > VOx/Al_2O_3. These results are confirmed by the relative reaction rates observed for the oxidation of ethane and the oxidation of ethylene. Microcalorimetry studies indicate that the heat of adsorption of both ethane and ethylene is the highest in the most selective MoVTeNb-M1 sample. Thus, the low olefin decomposition in the MoVTeNb-M1 catalyst is not due to weaker adsorption of ethylene but to the reduced ability of its active sites to activate ethylene. The same conclusion regarding the MoVTeNb-M1 catalyst can be drawn by FT-IR of adsorbed ethylene. On the other hand, NiSnOx active sites present a high overoxidation ability, as demonstrated by the notorious formation of oxygenated species, precursors of CO_x. However, the ethylene decomposition is rather mild because of the existence of many free Lewis sites not involved in the overoxidation reaction. In contrast, in the case of the VO_x/Al_2O_3 catalyst, almost all active sites are involved in the oxidation path, so that the olefins decompose readily.

1. Introduction

It is generally accepted that partial oxidation reactions are carried out by a Mars–van Krevelen mechanism [1,2]. However, other aspects must be also considered, such as the possible structure-sensitivity of catalytic reactions on oxides [3], the synergy of catalytic properties in oxide systems, the role of the monolayer in oxide catalysts, the dynamic state of oxide surfaces [4], or the mechanism of catalytic oxidation of hydrocarbons [5]. The role of oxygen species in hydrocarbon activation (i.e., electrophilicity and nucleophilicity of oxygen species in oxidation reactions) is especially remarkable [3]. In other words, "the surface of a solid is not a rigid static structure, on which various phenomena involving molecules adsorbed from the gas phase occur, but is always in dynamic interaction with the latter" [3]. On the other hand, concepts such as site isolation and phase cooperation [6] and multifunctionality of active sites [7] have subsequently led to the postulate of the "seven pillars" for the synthesis of oxidation reaction catalysts [8]. These concepts play an important role in the development of efficient catalysts for partial (amm)oxidation of both olefins [2] and alkanes [9].

Oxidative dehydrogenation (ODH) of alkanes is one of the partial oxidation reactions that have received the most attention in the last twenty years, because it could be a more sustainable alternative than the current, noncatalytic industrial process of olefin production (steam cracking of naphtha, liquefied petroleum gas [LPG], or ethane) [10–12]. Among the different alkanes (C_2–C_4), the ODH of ethane to ethylene is the one that currently generates

* Corresponding author.
E-mail address: jmlopez@itq.upv.es (J.M. López Nieto).

https://doi.org/10.1016/j.jcat.2021.07.015
0021-9517/

the best expectations for industrial application [13–17]. From comparison of the catalytic systems reported in the literature, three different catalysts for ethane ODH have been proposed in the past two decades, which correspond to the evolution of the most promising catalysts for this reaction [13–17]: (i) supported vanadium oxide, (ii) promoted nickel oxide, and (iii) multicomponent Mo–V–Te–Nb–O mixed metal oxides (Mo–V-based catalysts presenting orthorhombic molybdenum oxide bronze structure).

In the case of supported vanadium oxide catalysts, it is generally accepted that they should consist of rather acidic supports, with relatively high interaction of vanadium oxide with the supports. This is the case of γ-Al_2O_3-supported vanadium oxide catalysts [18–23], especially those with not very high vanadium loadings (ca. 1.4–4.2 V/nm^2), consisting of isolated vanadium species [20] that prevent the formation of bulk vanadium pentoxide [18–22]. In the best formulation, vanadia supported on alumina can partially mitigate ethylene overoxidation when compared with bulk vanadium pentoxide [18,20,21].

Promoted-nickel oxide catalysts can be considered a second group of active and selective catalysts for ethane ODH [24–26]. Nickel oxide alone is not appropriate to get high yields to ethylene, because it favors the direct formation of CO_2 from ethane. However, the addition of promoters, especially niobium (with Nb/Ni atomic ratios of ca. 0.03–020) [24], drastically changes the catalytic performance, greatly increasing the formation of the olefin at ethane conversions lower than 30%. Apparently, this improvement in the catalytic performance when suitable promoters, such as Nb, Sn, or Ti [24–30], are incorporated is due to the fact that the presence of appropriate metal oxides eliminates electrophilic oxygen species, which are highly active in CO_2 formation. In this way, by keeping nickel in its reduced valence state (Ni^{2+}), the number of O^- radicals that lead to combustion is limited [24,27,30,31]. The main difference between the catalytic performance of undoped and promoted NiO catalysts lies in the extent of the total oxidation of the alkane, rather than in the olefin formed. The first step in the mechanism is likely a concerted C–H activation [32] followed by a β-hydrogen elimination and subsequent release of ethylene and water.

Multicomponent Mo–V–Te(Sb)–Nb–O mixed oxide catalysts with a specific structure (the so-called M1 phase) were reported to show remarkably better behavior than the former vanadium-supported catalysts [33,34]. Their catalytic performance in ethane oxidation can be related to the presence of the multifunctional $Te_2M_{20}O_{57}$ (M = Mo, V, Nb) orthorhombic phase [35–40], in which V atoms are the active sites (the number of V atoms in the pure M1 phase is estimated to be ca. 1.8×10^{19} V-atoms g_{cat}^{-1} [37]). In addition, the presence of tellurium atoms in the framework of an orthorhombic bronze structure occupying the hexagonal channels facilitates the modification of acid sites on the catalyst surface, preventing the deep oxidation of both ethane and ethylene to carbon oxides [41–42]. These catalysts have been studied in recent years in order to improve catalytic activity [35–42]; however, the nature of active/selective species is not completely determined. It has been proposed that V-sites are the active ones [35–42], whereas the presence of Te-atoms could favor specific transformation of the catalyst structure, changing the characteristics of active sites and favoring higher selectivity to ethylene [44].

In this paper, the catalytic performance of representative catalysts of the last three groups for ethane and ethylene oxidation, that is, a multicomponent Mo–V–Te–Nb–O mixed metal oxide (with a Mo/V/Te/Nb atomic ratio of 1.0/0.25/0.17/0.17) [33], a Sn-doped NiO catalyst (with a Ni/Sn atomic ratio of 92/8) [28], and vanadium oxide supported on γ-Al_2O_3 (with 5 wt% of V-atoms) [18] is compared. The effect of surface Lewis acid sites on the adsorption enthalpy of ethane and ethylene in the different systems will be studied, correlating microcalorimetric with infrared spectroscopy (IR) studies, and the catalytic performance assessed by in situ IR studies where the reactivity of ethylene in the presence of molecular oxygen will be discussed, highlighting the role of surface oxygen species in the overoxidation of ethylene.

2. Experimental

2.1. Catalyst preparation

Some characteristics of the synthesized catalysts are shown in Table 1.

A multicomponent Mo–V–Te–Nb–O catalyst was prepared hydrothermally from aqueous gels of vanadyl sulfate, niobium oxalate, ammonium heptamolybdate, and telluric acid with a Mo/V/Te/Nb atomic ratio of 1/0.25/0.17/0.17 [35], which is slightly different from the composition of the final calcined catalyst (Table 1). The gel was transferred to a Teflon-lined stainless steel autoclave and kept at 175 °C for 48 h. The resulting precursor was filtered, washed, dried at 100 °C for 16 h, and heat-treated at 600 °C for 2 h under N_2. The M1 phase was further purified with a 15 wt% H_2O_2 aqueous solution for 2 h. This catalyst was named MoVTeNb-M1.

Sn-doped nickel oxide catalyst was prepared through the evaporation at 60 °C of a stirred ethanolic solution of nickel nitrate, $Ni(NO_3)_2{\cdot}6H_2O$ (Sigma–Aldrich), and tin oxalate, SnC_2O_4 (Sigma–Aldrich) [28]. Oxalic acid was added to the ethanolic solution with an additive/Ni molar ratio of 1.3, and a Ni/Sn atomic ratio of 92/8 was used. The paste obtained was dried overnight at 120 °C and finally calcined in static air for 2 h at 500 °C. This catalyst was named NiSnOx.

Vanadium oxide supported on γ-alumina catalyst was prepared by a wet impregnation method [18]. An ammonium metavanadate (Sigma–Aldrich) aqueous solution was adjusted at pH 7 with diluted

Table 1
Characteristics of catalysts.

Catalyst	VOx/Al_2O_3	NiSnOx	MoVTeNb-M1
Composition (at. ratio)	V:Al = 5.5:94.5	Ni:Sn = 92:8	Mo:V:Te:Nb = 63:16:11:11
V or Ni (wt.%)	5.0	66.9	5.9
S_{BET} (m^2 g^{-1})	144	84	8.8
V- or Ni- surface content (10^{18} atoms m^{-2})	4.0 [a]	8.7 [b]	1.8 [c]
Heat treatment	Air 550 °C (2 h)	Air 500 °C (2 h)	N_2 600 °C (2 h)
XRD crystalline phases detected	γ-Al_2O_3	NiO	M1
Other species present (Raman)	(VO_4) and $(VO_4)_n$ species	SnO_2 nanoparticles	–

[a] Assuming that the cross-sectional area of a molecule of supported V_2O_5 is 0.201 nm^2 [45], a monolayer of vanadium oxide completely covering the surface of the support should need 4.98×10^{14} molecules of V_2O_5 cm^{-2}.
[b] Assuming that a monolayer of nickel oxide completely covering the surface of the support should need 9.7×10^{14} molecules of NiO cm^{-2} [46], assuming a Ni/Sn atomic ratio of 92/8.
[c] As indicated in Ref. [37].

nitric acid and to this γ-Al_2O_3 (Suede-Chimie, S_{BET} = 188 m^2 g^{-1}) support was added. The amount of ammonium metavanadate used was adjusted to fix the vanadium content at 5 wt% V. This mixture was rotary evaporated under vacuum until a paste was obtained. This paste was dried overnight at 100 °C and finally calcined in static air for 6 h at 550 °C. This catalyst was named VOx/Al_2O_3.

2.2. Catalyst characterization

The chemical analysis of the solids was performed by inductively coupled plasma atomic emission spectrometry (ICP-AES).

The specific surface areas were determined by the Brunauer–Emmett–Teller (BET) method from N_2 adsorption isotherms at 77 K measured in a Micromeritics TriStar 3000 instrument.

X-ray diffraction (XRD) patterns of powder solids were collected with a PANalytical CUBIX instrument equipped with a graphite monochromator employing CuKα radiation (λ = 0.1542 mm) and operated at 45 kV and 4 mA. The distribution of the crystalline phases forming the catalysts was calculated by Rietveld refinement of the XRD patterns employing X'Pert Highscore Plus software.

Raman spectra were recorded with an "in via" Renishaw spectrometer equipped with an Olympus microscope. The samples were generally excited by the 514.5 nm line of an Ar^+ laser (Spectra Physics Model 171) with a laser power of 2.5 mW [47]. In the case of the NiO-based catalyst, the Raman spectrum was also obtained using a wavelength of 325 nm (UV-Raman) generated by a Renishaw HPNIR laser with a power of approximately 15 mW [49].

The adsorption enthalpy of hydrocarbons (ethane or ethylene) on the different catalysts was measured in separate experiments using a Sensys evo TG-DSC instrument from Setaram, equipped with a 3D thermal flow sensor. The sample (60–100 ± 1 mg) was treated in He flow (50 ml min^{-1}) at 5 °C min^{-1} up to 300 °C, kept for 30 min, and then cooled to 35 °C under He flow. After that, a mixture of ethane/He or ethylene/He (10% v/v) was flowed (10 ml min^{-1}) onto the catalyst at 35 °C until no variations in mass or heat flow were detected. The exothermic peaks corresponding to the adsorption were integrated to provide the total enthalpy of adsorption. The mean adsorption energy for each hydrocarbon was calculated by considering the total amount of hydrocarbon adsorbed.

IR spectra of adsorbed CO were recorded at low temperature (-165 °C) with a Bruker Vertex 70 spectrometer using a DTGS detector and acquired at 4 cm^{-1} resolution. An IR cell allowing in situ treatments in controlled atmospheres and temperatures from −165 to 500 °C has been connected to a vacuum system with a gas dosing facility. For IR studies, the samples were pressed into self-supported wafers and treated at 250 °C in oxygen flow (10 ml min^{-1}) for 1.5 h, followed by evacuation at 10^{-4} mbar at the same temperature for 1 h. After activation, the samples were cooled to −165 °C under dynamic vacuum conditions, followed by CO dosing at increasing pressure (0.4–8.5 mbar). IR spectra were recorded after each dosage.

IR spectra of NH_3 adsorption were recorded with a Thermo "is50" spectrometer using a DTGS detector and acquired at resolution 4 cm^{-1}. A homemade glass IR cell allowing in situ treatments in controlled atmospheres and temperatures from 25 to 500 °C was connected to a vacuum system with a gas dosing facility. The samples were preactivated as before, at 250 °C in oxygen flow for 1.5 h followed by evacuation at 10^{-4} mbar at the same temperature for 1 h. After the activation, the samples were cooled to 25 °C under dynamic vacuum conditions and then dosed with NH_3 at increasing pressure (0.4–25 mbar) until saturation, followed by evacuation at the same temperature. Afterwards, the temperature was increased to 100 °C under vacuum. IR spectra were recorded after each dosage and then after each evacuation temperature.

In the in situ IR experiments, after sample activation under conditions similar to those in the IR-CO experiments, 43 mbar ethylene and 84 mbar O_2 were coadsorbed at 25 °C. Then the cell was closed and the temperature was increased stepwise to 100, 150, 200, and 250 °C at constant pressure. At each temperature the sample was maintained for 30 min. IR spectra were recorded after each temperature on the "hot" and "cooled down" pellet.

2.3. Catalytic tests

The catalytic experiments were carried out under steady state conditions using a fixed-bed quartz tubular reactor (i.d. 20 mm, length 400 mm) equipped with a coaxial thermocouple for catalytic bed temperature profiling, working at atmospheric pressure in the temperature range 350–450 °C. The flow rate (25–100 ml m in^{-1}) and the amount of catalyst (0.5–2.0 g, particle size 0.3–0.5 mm) were varied to achieve different ethane conversion levels. In all cases, silicon carbide was used to avoid hot spots (SiC/catalyst weight ratio 3). The feed consisted of a mixture of hydrocarbon/oxygen/helium with molar ratio 5/5/90 (using ethane or ethylene) or CO/air with molar ratio 0.5/99.5. Reactants and reaction products were analyzed by online gas chromatography using two columns [44]: (i) Porapak QS (2.0 m × 1/8 in.) and ii) (ii) Carbosieve-S (2.5 m × 1/8 in.).

3. Results and discussion

3.1. Characterization of catalysts

Table 1 shows the characteristics of catalysts. The V- or Ni-surface content in each catalytic system has been also calculated by considering previously reported data on similar types of catalysts (see footnotes in Table 1) [37,45,46].

The XRD pattern of the multicomponent Mo–V–Te–Nb–O mixed metal oxides catalyst (MoVTeNb-M1) is characterized by the presence of diffraction peaks related to the $(TeO)_2M_{20}O_{56}$ structure [JCPDS: 18–582], the so-called M1 phase [35–41] (Fig. S1A in the Supporting Information). The corresponding Raman spectrum, using the 514 nm wavelength excitement laser, showed an intense band at ca. 872 cm^{-1} with a broad shoulder in the 770–840 cm^{-1} region and a signal at 477 cm^{-1}. These signals could correspond to asymmetric and symmetric stretching modes of the Me–O–Me bonds, respectively (Fig. S1B). Moreover, a weak shoulder can be seen at ca. 980 cm^{-1}, assigned to stretching vibrations of terminal Mo=O and V=O [47] and a band at ca. 664 cm^{-1} that, along with the broad band at ca. 820 cm^{-1}, is assigned to the Nb–O–Nb bonds [48]. All these signals confirm the main presence of the M1 phase [47]. Furthermore, the XPS of the vanadium $2p_{3/2}$ core level is included in Fig. S1C. A unique symmetrical signal at ca. 515.2 eV is observed, suggesting the single presence of V^{4+} species [33].

SnO_2–doped NiO catalyst (NiSnOx), with a Ni/Sn atomic ratio of 92/8, presents a surface area of 84 m^2 g^{-1} and a typical X-ray diffraction pattern characterized by the presence of NiO crystallites (JCPDS: 78-0643) with the presence of a minority of SnO_2 (JCPDS 41-1445) (Fig. S2A) [28]. Visible Raman spectra (514 nm) of this catalyst are characterized by the presence of a broad band at ca. 516 cm^{-1}, suggesting some modification of NiO crystallites [49] (Fig. S2B). In addition, the UV-Raman spectrum (325 nm) of the NiSnOx catalyst confirms the presence of NiO nanoparticles [50], with the presence of five bands that correspond to one-phonon LO modes (at 516 and 580 cm^{-1}), two-phonon 2TO modes (at 707 cm^{-1}), TO + LO modes (at ~ 906 cm^{-1}), and 2LO modes (at ca. 1109 cm^{-1}). On the other hand, the visible Raman spectrum for this catalyst presents a broad single band at ca. 516 cm^{-1}, as observed in other promoted NiO catalysts [49]. In addition,

Fig. S2C shows the Ni2$p_{3/2}$ core-level spectrum, in which the characteristic peaks for NiO can be seen with a main signal at ca. 853.7 eV, along with a broad satellite (Sat II) at ca. 860.9 eV, both associated with Ni^{2+} species, and a second signal (Sat I) at higher binding energy (855.7 eV) than that of the main one, which is related to the presence of defects such as Ni^{3+}, Ni^{2+} vacancies or Ni^{2+}–OH species [28,30].

γ-Al_2O_3-supported vanadium oxide catalyst (VOx/Al_2O_3), with a surface area of 146 m^2 g^{-1}, presents a typical X-ray diffraction pattern of the pure support with no apparent presence of vanadium pentoxide crystallites (Fig. S3A), which suggest that vanadium species are highly dispersed on the surface of the support [18]. This is also confirmed by Raman spectroscopy (Fig. S3B), which shows a band at ca. 927 cm^{-1} (broad band 920–940 cm^{-1} in UV-Raman) in agreement with good dispersion of polymeric vanadium species onto the alumina surface [51]. In any case, both UV and visible Raman spectra confirm the absence of V_2O_5 crystallites. In addition to this, XPS analysis of the vanadium 2$p_{3/2}$ core level showed an asymmetric signal centered at ca. 516.5 eV (Fig. S3C), suggesting the main presence of V^{5+} [52]. However, the minority presence of V^{4+} species, with binding energy at 514.5 eV, should be also considered.

Fig. 1 presents the TPR patterns of catalysts. For the MoVTeNb-M1 sample, two reduction peaks, at ca. 500 and 520 °C, are observed. The first reduction peak is related to the reduction of V–O–Mo pairs at the surface of the catalyst, whereas the second reduction peak is related to the reduction of bulk [35,53].

However, a single reduction peak, with the maximum H_2-consumption at ca. 320 and 475 °C, respectively has been observed in the cases of NiSnOx and VOx/Al_2O_3 catalysts. They are related to the consecutive reduction in each catalytic system, ($NiO \rightarrow Ni^{\delta+} \rightarrow Ni^0$ [28,54] and $V^{5+} \rightarrow V^{4+} \rightarrow V^{3+}$) [18,55]. We must indicate that surface and bulk reduction is observed for MoVTeNb-M1 and NiSnOx catalysts, whereas only the surface vanadium species of the catalyst are reduced in VOx/Al_2O_3.

The amount of adsorbed hydrocarbons and the heat of adsorption of ethane and ethylene, measured by microcalorimetry, are summarized in Table 2. From our calorimetric experiments, we can assume that high surface coverage occurs; thus, all adsorption sites, strong and weak, are covered. MoVTeNb-M1 shows the highest heat of adsorption, 32 kJ mol^{-1}; with ethylene interacting slightly more strongly than ethane (a value of 39 kJ mol^{-1} is obtained in this case), which is in good agreement with previous results [37]. The adsorption enthalpy of both ethane and ethylene on VOx/Al_2O_3 and NiSnOx catalysts results in low heat values of 10–13 kJ mol^{-1}, which are close to the condensation of the hydrocarbon molecules [37]; there is no apparent strong interaction of these hydrocarbons with the surfaces of VOx/Al_2O_3 and NiSnOx catalysts.

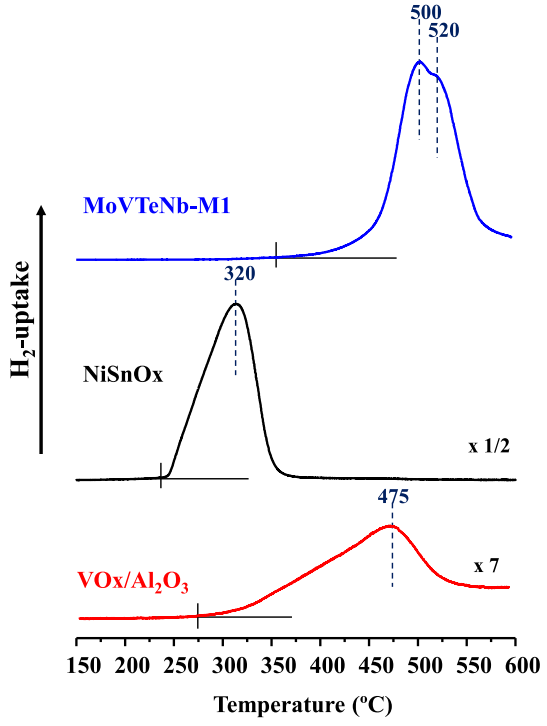

Fig. 1. TPR H_2 results of catalysts: (a) MoVTeNb-M1, (b) NiSnOx, and (c) VOx/Al_2O_3.

The amount of adsorbed hydrocarbon (ethane and ethylene) on MoVTeNb-M1 is about half that determined for VOx/Al_2O_3 and NiSnOx catalysts (Table 2). For a more proper comparison of the amount of adsorbed hydrocarbons on the different catalysts, the measured amount was normalized to the specific surface area. The density of active surface sites for the ethane adsorption follows the order MoVTeNb-M1 (4.9 μmol_{C2H6} m^{-2}) > NiSnOx (1.8 μmol_{C2H6} m^{-2}) > VOx/Al_2O_3 (0.8 μmol_{C2H6} m^{-2}). They are similar to those observed by the ethylene adsorption: MoVTeNb-M1 (5.3 μmol_{C2H4} m^{-2}) > NiSnOx (1.5 μmol_{C2H4} m^{-2}) > VOx/Al_2O_3 (0.8 μmol_{C2H4} m^{-2}). Note that the surface density of sites for ethylene and ethane adsorption is kept in a similar range for each catalyst.

IR spectra of CO adsorption as probe molecule for surface Lewis acid titration performed at −165 °C are shown in Fig. 2A. In the case of the VOx/Al_2O_3 sample, a weak band at 2185 cm^{-1}, associated with V^{4+} ions, together with a more intense band at 2157 cm^{-1}, due to CO coordinated with hydroxyl groups of the Al_2O_3 support, is observed [56].

The NiSnOx sample shows a markedly higher density of Lewis acid sites, whose carbonyl frequency is slightly red-shifted, ascribed to a lower acid strength (2174 cm^{-1}). This IR band has been ascribed to Ni^{2+} [57] and/or Sn^{4+} [58]. In addition, for CO coordinated to hydroxyl groups, a band at 2151 cm^{-1} is detected. Notoriously, for the MoVTeNb-M1 sample, only one peak at 2131 cm^{-1} is observed, which may be related to CO bound to reduced Mo and/or V species, characterized by π back-donation shifting the ν(CO) to lower values [59] or to physisorbed CO inside the hexagonal channels of the M1 structure.

The acidity of the catalysts has been also studied by IR NH_3, and the spectra are displayed in Fig. 2B. In our study, NH_3 is adsorbed at RT and further desorbed at 25 °C (Fig. 2B) and 100 °C (Fig. S4). At 25 °C, strong IR bands are observed in the MoVTeNb-M1 sample (blue line) located at 1650, 1601, 1420, 1265, and 1197 cm^{-1}. According to the literature [59,60], ammonia coordinated on Lewis sites gives characteristic bands at 1601 ($\delta_{as}NH_3$) and 1265 and 1197 cm^{-1} (splitting of the symmetric deformation mode, δ_{sym}-NH_3), while ammonium cations (NH_4^+) formed by coordination of

Table 2
Comparative results of microcalorimetric measurements.[a]

Catalyst	Hydrocarbon (HC)	Heat (J/g_{cat})	Adsorbed HC μmol/g_{cat}	Heat of adsorption (kJ/mol_{HC})
MoVTeNb-M1	Ethane	1.546	48.6	32
MoVTeNb-M1	Ethylene	2.072	53.3	39
VOx/Al_2O_3	Ethane	1.334	110.7	12
VOx/Al_2O_3	Ethylene	1.184	122.9	10
NiSnOx	Ethane	2.004	154.1	13
NiSnOx	Ethylene	1.299	124.8	10

[a] Experiments undertaken at 35 °C.

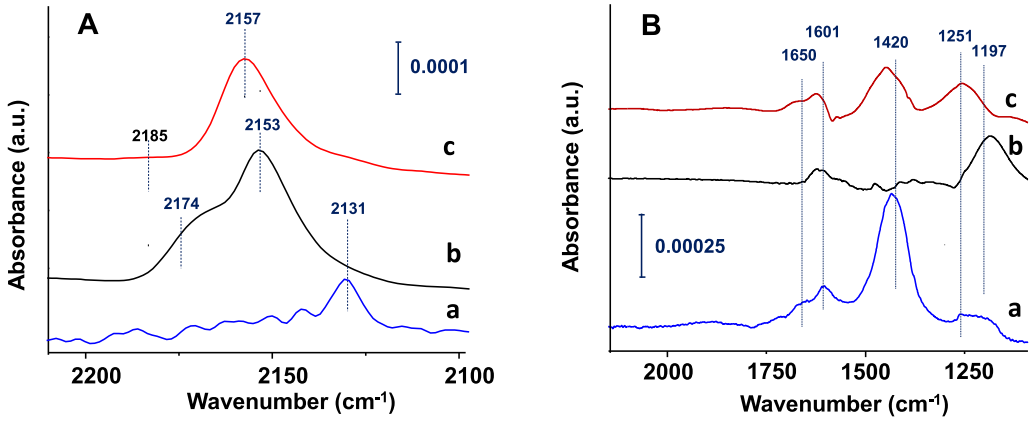

Fig. 2. IR spectra of CO adsorption (A) at saturation coverage at −165 °C and IR spectra of NH_3 adsorption (B) at an evacuation temperature of 25 °C, on MoVTeNb-M1 (a); NiSnOx (b); and VOx/Al_2O_3 (c). IR spectra have been normalized to the sample weight and surface area.

NH_3 with Brønsted acid sites give rise to the bands at 1420 and 1650 cm^{-1}.

Thus, both Lewis and Brønsted sites can be envisaged in the MoVTeNb-M1 sample. Notice that Brønsted acid sites have not been detected in the respective IR-CO spectra, probably due to its small amount and the higher sensitivity of NH_3 to Brønsted titration. In contrast, a markedly lower density of acid sites is observed in the VOx/Al_2O_3 (green line), based on the lower intensity of the above-reported IR bands [60]. In the case of the NiSnOx sample (black line), a careful analysis of the IR shows the formation of hydrazine on the catalyst surface (IR bands at 1629, 1560, 1363, 1259, and 1185 cm^{-1}), which may come about by the oxidation of ammonia. This is not surprising, due to the highly oxidizing character of the sample.

When the desorption temperature is increased to 100 °C (Fig. S4), IR bands in all samples decrease in intensity, while a clear differentiation can still be observed among the catalysts, where MoVTeNb-M1 contains the highest density of acid sites, followed by VOx/Al_2O_3 and NiSnOx, the last one behaving as a redox catalyst. The fact that the IR bands of adsorbed NH_3 decrease around 89% after the temperature is increased to 100 °C indicates low acid strength of the acid sites, in agreement with previous work [41,60].

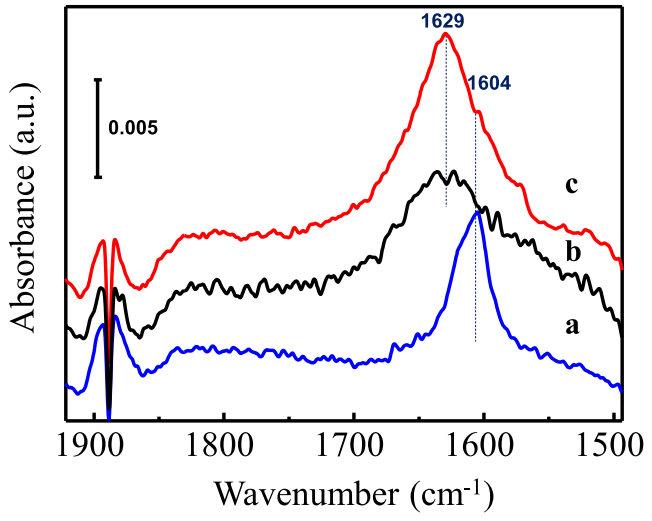

Fig. 3. IR spectra of 43 mbar of ethylene adsorbed at 25 °C on MoVTeNb-M1 (a), NiSnOx (b), and VOx/Al_2O_3 (c). The IR band in the range 1600–1630 cm^{-1} corresponds to ν(C = C). IR spectra have been normalized to the sample weight.

To correlate the strength of surface Lewis acid sites with the previous microcalorimetric studies, IR studies of ethylene adsorption have been performed. A band in the range 1600–1630 cm^{-1} can be related to the presence of ν(C = C) of ethylene adsorbed on the surface of the catalyst [61]. This band has been observed for all the catalysts, as shown in Fig. 3. However, the ν(C = C) of ethylene is red-shifted in the MoVTeNb-M1 sample (IR band at 1604 cm^{-1}) from that of the NiSnOx (~1629 cm^{-1}) and VOx/Al_2O_3 (~1629 cm^{-1}) samples, indicating a higher interaction strength between the olefin group and the Lewis acid site in the MoVTeNb-M1 sample, in agreement with the higher heat of adsorption determined by microcalorimetry.

3.2. Catalytic results

The catalytic performance of these catalysts (i.e., MoVTeNb-M1, NiSnOx, and VOx/Al_2O_3) in the oxidative dehydrogenation (ODH) of ethane and in the oxidation of ethylene has been studied comparatively at a fixed and relatively low reaction temperature (in the temperature range 350–450 °C), maintaining the same hydrocarbon/O_2/He molar ratio 5/5/90 and modifying the contact time by changing the catalyst weight and/or the total flow. In this way we can observe the evolution of the selectivity to the main reaction products when the ethane conversion increases. A summary of the catalytic results in the ODH of ethane on these catalysts is shown in Table 2. We must note that other experiments were undertaken using different reactant concentrations in order to determine the reaction orders referred to oxygen and to hydrocarbon.

The reactivity of the multicomponent Mo–V–Te–Nb–O mixed metal oxide catalysts, presenting mainly M1, is likely due only to the reactivity of the vanadium sites in a suitable environment [33–44]. In fact, it is known that molybdenum oxide-based catalysts can activate ethane at temperatures over 500 °C [19], which are much higher than the reaction temperature of the present work, whereas tellurium and niobium sites are inert under these reaction conditions. The reaction rate of ethane transformation per mass of catalyst (r_{C2H6}) is 2.29 $mmol_{C2H6}\ g_{cat}^{-1}h^{-1}$, whereas the rate per mass of active site (vanadium) is 38.8 $mmol_{C2H6}\ g_V^{-1}h^{-1}$.

The reactivity of the VOx/Al_2O_3 catalyst is due to the vanadium sites and depends on both the reducibility of the catalyst and the subsequent reoxidation of the reduced catalyst [20,55], since at the reaction temperature used in this work, the reactivity of pure γ-Al_2O_3 has been shown to be negligible. The reaction rate of ethane transformation per mass of catalyst (r_{C2H6}) is 0.424 $mmol_{C2H6}\ g_{cat}^{-1}h^{-1}$ (Table 2), whereas the rate per mass of active site (vanadium) is ca. 13.7 $mmol_{C2H6}\ g_V^{-1}h^{-1}$.

The reactivity of the NiSnOx catalyst is due to the nickel sites [24–30], as the tin sites are inactive in ethane activation under these reaction conditions [28]. Thus, in this case, the reaction rate of ethane transformation per mass of catalyst (r_{C2H6}) is 17.6 $mmol_{C2H6}\ g_{cat}^{-1}h^{-1}$ whereas the rate per mass of active site (nickel) is 26.3 $mmol_{C2H6}\ g_{Ni}^{-1}h^{-1}$.

Accordingly, the reaction rate for ethane oxidation (r_{C2H6}) during ethane ODH at 400 °C decreases according to the following trend: NiSnOx (17.6 $mmol_{C2H6}\ g_{cat}\ h^{-1}$) > MoVTeNb-M1 (2.29 $mmol_{C2H6}\ g_{cat}\ h^{-1}$) > VOx/Al_2O_3 (0.68 $mmol_{C2H6}\ g_{cat}\ h^{-1}$) (Table 3).

Fig. 4 shows the variation of the selectivity to ethylene with the ethane conversion at 400 °C (data obtained by varying the contact time). By comparing the variation of the selectivity to ethylene with ethane conversion at 400 °C, it can be concluded that ethane conversion has a very low influence on the selectivity to ethylene when the reaction is carried out over multicomponent MoVTeNb-M1 catalysts, with selectivity to ethylene higher than 90% for ethane conversion up to 80%. However, a higher influence of ethane conversion on the selectivity to ethylene is observed for NiSnOx and especially for VOx/Al_2O_3 catalyst.

Table 3
Catalytic data in ethane and ethylene oxidation on representative catalysts.[a]

Catalyst	VOx/Al_2O_3	NiSnOx	MoVTeNb-M1
Ethane ODH			
Reaction rate of ethane consumption ($mmol_{C2H6}\ g_{cat}^{-1}h^{-1}$)	0.68	17.6	2.29
Reaction rate of ethane consumption per active site ($mmol_{C2H6}\ g_{active\ site}^{-1}h^{-1}$)	13.7	26.3	38.8
Reaction rate of ethane consumption per surface area ($mmol_{C2H6}\ m^{-2}h^{-1}$)	0.09	0.31	6.8
Reaction rate of ethylene formation ($mmol_{C2H4}\ g_{cat}^{-1}h^{-1}$)	0.42	14.9	2.27
TOF($10^4\ s^{-1}$)[b]	1.97	40.3	242
$n(C_2H_6)$ in ethylene formation[c]	0.80	0.52	0.88
$n(O_2)$ in ethylene formation[c]	0.15	0.26	0.22
Ethylene oxidation			
Reaction rate of ethylene consumption, ($mmol_{C2H4}\ g_{cat}^{-1}h^{-1}$)	1.76	3.71	0.17
Reaction rate of ethylene conversion per active site ($mmol_{C2H4}\ g_{active\ site}^{-1}h^{-1}$)	35.2	5.55	2.81
Reaction rate per surface area ($mmol_{C2H4}\ m^{-2}h^{-1}$)	0.24	0.07	0.50
TOF($10^4\ s^{-1}$)[b]	5.07	8.49	18.0
Relative reactivity ethylene/ethane	2.58	0.21	0.072

[a] Reaction temperature = 400 °C; hydrocarbon/O_2/He = 5/5/90 (molar ratio); reaction rates were determined for conversions lower than 5%.
[b] Determined considering the V- or Ni- surface content from Table 1.
[c] Reaction order in the ethylene formation during the ethane oxidation $r = kP_{C2H6}^{n(C2H6)}p_{O2}^{n(O2)}$.

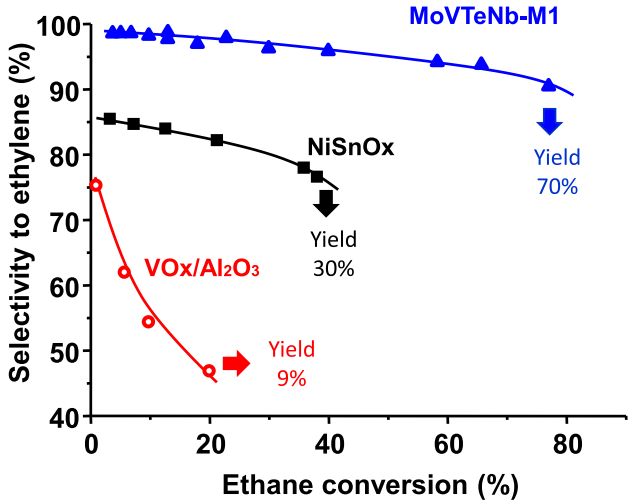

Fig. 4. Variation of the selectivity to ethylene with the ethane conversion at 400 °C in the ODH of ethane. Catalysts: MoVTeNb-M1 (▲), NiSnOx (■), VOx/Al_2O_3 (●). Remaining reaction conditions in text. Detailed data of representative catalysts are shown in Table S1.

Considering the density of V or Ni in the surface, TOF values have been estimated. It is noteworthy that the M1 catalyst presents the highest value for ethane activation, followed by the NiSnOx catalyst, the VOx/Al_2O_3 catalyst presenting the lowest values. In any case, these values must be taken with care, as the determination of true active sites in the surface in these complex structures is not straightforward.

In the ODH of ethane on multicomponent MoVTeNb-M1 catalyst, three reaction products have been observed, ethylene (mainly) and CO and CO_2 (as minority), whereas acetic acid was not observed (Table S1). Initially, the ethane is transformed into ethylene, as its initial selectivity to ethylene is ca. 100% (Fig. 4). Interestingly, the selectivity to ethylene hardly decreases with ethane conversion (from 99% at 2% ethane conversion to 96% at 40% ethane conversion). In addition, no influence of reaction temperature on selectivity to ethylene is observed on this catalyst in the range 350–450 °C (Fig. S4).

In an opposite trend, a drastic decrease of the selectivity to ethylene is observed on VOx/Al_2O_3 catalyst when the ethane conversion increases. Thus, VOx/Al_2O_3 catalyst presents an initial selectivity to ethylene of ca. 80% (at 400 °C) or 90% at (450 °C), whereas both CO (initial selectivity of ca. 16% or 6% at 400 or 450 °C, respectively) and CO_2 (initial selectivity ca. 4% regardless of the reaction temperature) can also be formed directly from ethane (Fig. S4).

It is noteworthy that the selectivity achieved over the alumina-supported vanadium oxide catalyst presented here is even slightly lower than that over other vanadia/alumina catalysts reported in the literature [20,55]. However, this is related to the low reaction temperature used in the present study, in contrast with typical reaction temperatures of 500–550 °C reported elsewhere [18–20], and the strong influence of reaction temperature on selectivity to ethylene [20], in part as a consequence of changes in the reducibility and reoxidation of the catalyst [55].

Intermediate behavior is observed over the Sn-doped NiO catalysts (NiSnOx). Most of the ethane is transformed into the olefin, with an initial selectivity to ethylene of 85–90% being achieved (Fig. 4). However, a slight decrease of the selectivity to ethylene is observed when the ethane conversion increases (from 86% at 2% ethane conversion to 76% at 40% ethane conversion), but a greater influence of the ethane conversion on the selectivity to ethylene is observed for higher ethane conversion. In addition, only two reaction products (ethylene and CO_2) have been observed during the ODH of ethane over NiSnOx catalyst. Nevertheless, no influence of reaction temperature on selectivity to ethylene is observed between 400 and 450 °C (Fig. S4).

On the other hand, the catalysts have been tested in the oxidation of ethylene (Table S2) and the selectivity to the main reaction products is presented in Fig. 5.

In the oxidation of ethylene over MoVTeNb-M1 or VOx/Al_2O_3 catalysts two reaction products (CO and CO_2) have been observed (Fig. 5 and Table S2), although acetic acid was also detected, as traces, over VOx/Al_2O_3. In both cases, the selectivity to carbon oxides remained constant with the ethylene conversion, suggesting that there has not been appreciable CO oxidation to CO_2. However, only CO_2 was identified during the ethylene oxidation over NiSnOx catalyst (Fig. 4): neither CO nor acetic acid was detected.

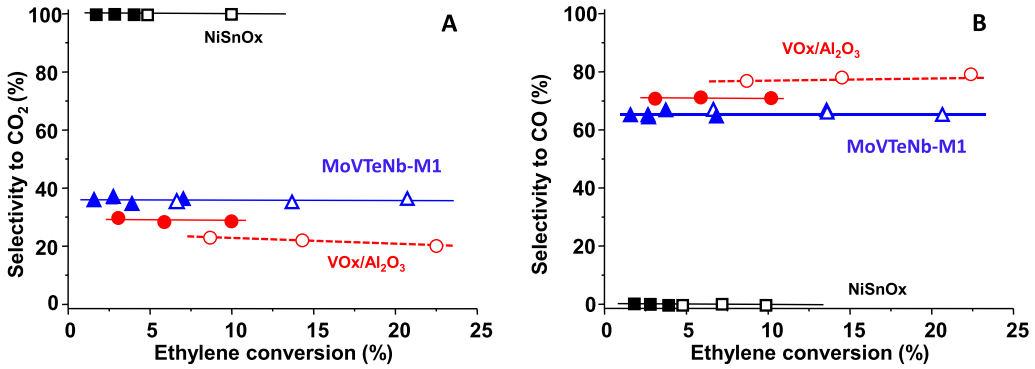

Fig. 5. Variation of the selectivity to CO and CO_2 with the ethylene conversion at 400 (●, ▲, ■) and 450 °C (○, △, □,) during the oxidation of ethylene over MoVTeNb-M1 (▲, △), NiSnOx (■, □), and VOx/Al_2O_3 (●, ○) catalysts. Reaction conditions in *Experimental*.

The reaction rate of ethylene transformation per mass of catalyst during the ethylene oxidation at 400 °C (r_{C2H4}) decreased according to the following trend: NiSnOx (3.71 $mmol_{C2H6}\ g_{cat}^{-1}h^{-1}$) > VOx/Al_2O_3 (1.76 $mmol_{C2H4}\ g_{cat}^{-1}h^{-1}$) > MoVTeNb-M1 (0.166 $mmol_{C2H6}\ g_{cat}^{-1}h^{-1}$). However, the rate of ethylene transformation per mass of active site (vanadium or nickel) decreased as follows: VOx/Al_2O_3 (35.2 $mmol_{C2H4}\ g_V^{-1}h^{-1}$) > NiSnOx (5.55 $mmol_{C2H6}\ g_{Ni}^{-1}h^{-1}$) > MoVTeNb-M1 (2.81 $mmol_{C2H6}\ g_V^{-1}h^{-1}$).

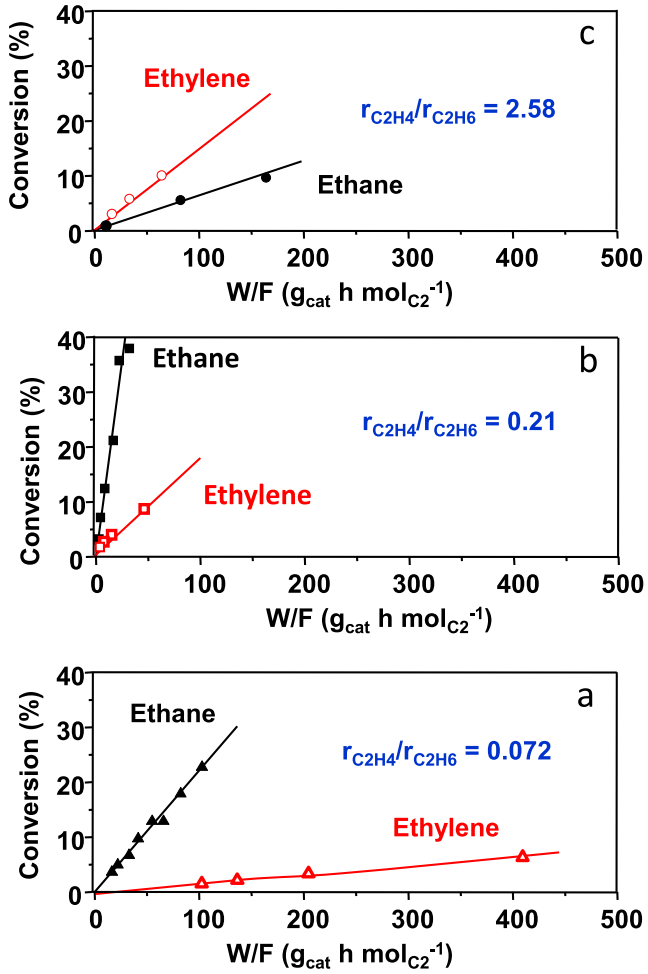

Fig. 6. Variation of the ethane and ethylene conversion with contact time, W/F, during the oxidation of ethane and ethylene over MoVTeNb-M1 (a), NiSnOx (b), and VOx/Al_2O_3 (c) catalysts. Reaction conditions: 400 °C, C_2/O_2/He molar ratio 5/5/90 (for ethane or ethylene).

Fig. 6 shows the variation of ethane or ethylene conversion with contact time during their oxidation over MoVTeNb-M1 (Fig. 6a), NiSnOx (Fig. 6b), and VOx/Al_2O_3 (Fig. 6c) catalysts at 400 °C. The corresponding r_{C2H4}/r_{C2H6} ratios achieved for each catalytic system have been also included. These reaction rates have been calculated for hydrocarbon conversions lower than 5%.

The reactivity of the MoVTeNb-M1 catalyst in olefin transformation was ca. 15 times lower than that in the ethane transformation (Fig. 6a), which is in agreement with the extremely low drop in the selectivity to ethylene observed during the ODH of ethane (Fig. 4). On the other hand, the reactivity of NiSnOx catalyst in ethylene oxidation was low, only around 1/5 of the reaction rate observed in the alkane transformation (Fig. 6b), which can explain the slow drop in the selectivity to ethylene observed during the ODH of ethane (Fig. 4). However, in the case of the VOx/Al_2O_3 catalyst, its catalytic activity in ethylene transformation was 2–3 times higher than that in the ethane transformation (Fig. 6c), which is in agreement with the important drop in the selectivity to ethylene observed during the ODH of ethane (Fig. 4).

Furthermore, in previous comparative studies of undoped and Zr- or Nb-doped NiO catalysts for ethane ODH at 350 °C, it was observed that the r_{C2H4}/r_{C2H6} ratio shows small differences between 0.41 and 0.53 [62], similar to that reported here. However, supported vanadium oxide catalysts present r_{C2H4}/r_{C2H6} ratios between 2 and 10, depending on the hydrocarbon feed and the support [16].

The results presented here clearly explain the higher selectivity to ethylene achieved during the ODH of ethane over MoVTeNb-M1 catalysts and the lower selectivity to ethylene achieved during the ODH of ethane over VOx/Al_2O_3 catalysts, whereas Me-doped nickel oxide catalysts present intermediate selectivity to ethylene. Accordingly, for ethane ODH, the selectivity to ethylene on these catalysts strongly depends on the relative reaction rates for ethane and ethylene oxidation.

Further experiments undertaken in the oxidation of CO (Fig. 7) showed that at the temperature of this study, carbon monoxide was hardly transformed into carbon dioxide over MoVTeNb-M1 and VOx/Al_2O_3 catalysts, which is in agreement with the null CO oxidation observed in the ethylene oxidation.

However, total conversion of CO into CO_2 was observed at the temperature of this study over NiSnOx catalyst (Fig. 7). Even more, at temperatures of ca. 125 °C below the reaction temperature of this study, the CO conversion had already reached 100%. This is in agreement with the fact that CO was not observed in neitherethane ODH nor ethylene oxidation reactions over NiSnOx catalyst, as CO quickly transforms into CO_2. These results are in agreement with those previously reported, in which the catalytic activity for CO oxidation can be explained by the ability to show

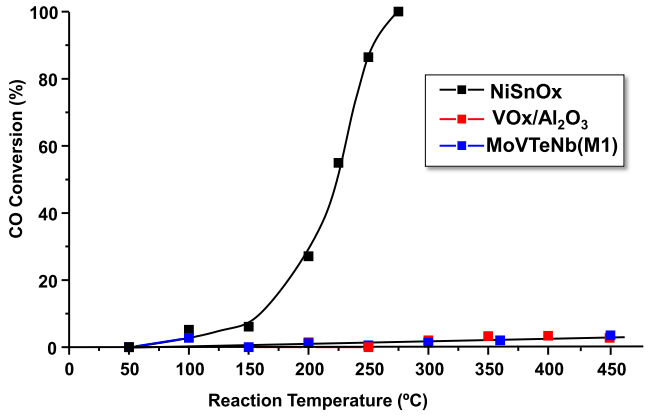

Fig. 7. Variation of the oxidation of CO with reaction temperature over MoVTeNb-M1, NiSnOx, and VOx/Al_2O_3 catalysts. Reaction conditions: 0.5 mol.% CO in synthetic air; 0.1 g of catalyst; total flow 50 ml min^{-1}.

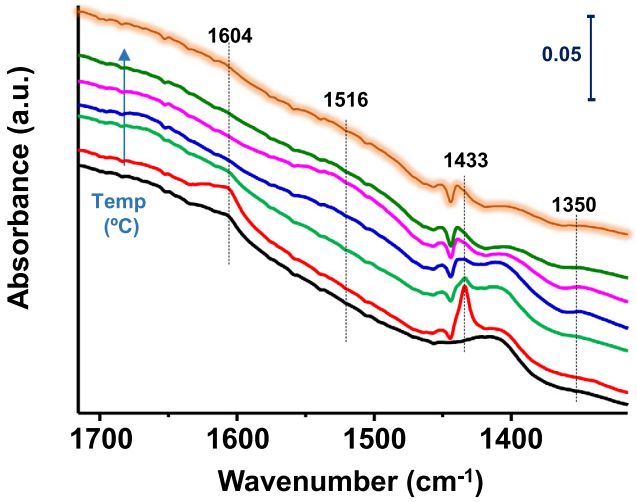

Fig. 8. IR spectra of the coadsorption of 43 mbar ethylene and 84 mbar O_2 on MoVTeNb-M1 catalyst and increasing reaction temperatures at constant reaction pressure (~128 mbar): 25 °C (red); 100 °C (green); 150 °C (blue); 200 °C (magenta); 250 °C (dark green). Cooling to 25°C (highlighted orange line). In black, reference spectrum prior to ethylene adsorption. (For interpretation of the references to colour in this figure legend, the reader is referred to the web version of this article.)

homomolecular exchange of oxygen, which strongly depends on the presence/absence and strength of Me=O bonds [63]. In this way, undoped and Sn-doped NiO catalysts present rates of homomolecular exchange of oxygen [28] higher than those achieved for MoVTeNbO mixed oxides [47] or supported vanadium oxide [64] catalysts. However, there is no parallelism between the catalytic activity of catalysts for CO oxidation (Fig. 7) and the selectivity to ethylene during ethane ODH (Fig. 4).

According to these catalytic results, a general pathway can be proposed for the ODH of ethane on both MoVTeNb-M1 and VOx/Al_2O_3 catalysts (Scheme 1a), although values of kinetic constants strongly depend on the characteristics of catalysts.

Ethane is initially transformed into ethylene (mainly), CO, and CO_2. In addition, the ethylene formed is slowly (MoVTeNb-M1 catalyst) or quickly (VOx/Al_2O_3 catalyst) oxidized into CO (mainly) and CO_2, whereas the CO formed is not transformed into CO_2.

On the other hand, a slightly different pathway can be proposed for the ODH of ethane on NiSnOx catalyst (Scheme 1b). Ethane is directly transformed into ethylene (mainly) and CO_2, whereas the ethylene formed oxidizes into CO_2. In spite of the nondetection of CO, the appearance of CO as a reaction intermediate in CO_2 formation is highly likely.

3.3. Infrared study of adsorbed ethylene

To obtain fundamental knowledge of the processes taken place on the catalyst surface, in situ IR studies of ethylene and O_2 coadsorption have been performed at increasing reaction temperatures from 25 to 250 °C (Figs. 8 and 9).

In the MoVTeNb-M1 sample (Fig. 8) fast desorption of ethylene is observed at 100 °C (depletion of the IR band at 1605 cm^{-1}), followed by the absence of an additional IR signal at increasing temperature, except for a broad band at 1516 and 1350 cm^{-1} (related to carboxylate species, ν_{asym} and ν_{sym}, respectively), indicating the practical nonexistence of surface-catalyzed reaction between ethylene and oxygen, in agreement with the high selectivity of this catalyst in the ODH of ethane. After the IR sample cools from 250 to 25 °C, no changes in the spectrum are observed, indicating the absence of reaction during the experiment.

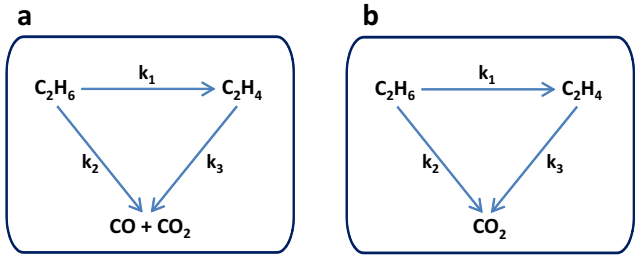

Scheme 1. Reaction scheme for the oxidative dehydrogenation of ethane on (a) MoVTeNb-M1 or VOx/Al_2O_3 catalysts; (b) NiSnOx catalyst.

In the NiSnOx sample (Fig. 9A), ethylene is desorbed at 100 °C and new IR bands appear at 1576, 1511, 1345, and 1304 cm^{-1}, associated with carbonate/carboxylate species, growing in intensity with increasing temperature. This means a high reactivity of oxygen species resulting in the formation of oxygenated species, precursors of CO_x. Interestingly, after the IR sample cools from 250 to 25 °C, readsorption of nonreacted ethylene (IR bands at 1629, 1375, and 1214 cm^{-1}) [65] is observed, indicating the existence of free Lewis sites not involved in the overoxidation reaction.

Finally, in the VOx/Al_2O_3 sample (Fig. 9B), ethylene is desorbed at 100 °C, and until 200 °C, no new IR bands are observed. The new bands, which appear at 1548 and 1388 cm^{-1}, together with bands at 1462 and 1302 cm^{-1} formed at 250 °C, are all due to carbonate species. In contrast with the previous sample, readsorption of ethylene on the cooled sample is markedly lower, visualized by a small shoulder at 1629 cm^{-1}, indicating that almost all sites are involved in the oxidation path.

This fact may explain the drastic decrease in selectivity to ethylene observed on the VOx/Al_2O_3 sample when ethane conversion increases, while this behavior is not observed on the NiSnOx sample. In this last case, the coexistence of free Lewis sites not involved in the oxidation process may favor the ethane dehydrogenation path.

Interestingly, the different IR patterns observed on the different samples, which should be related to the reactivity of surface oxygen species, agree with the TPR data. Thus, the reducibility of active sites is higher on the NiSnOx sample (reduction temperature at 350 °C) than on VOx/Al_2O_3 (reduction temperature 480 °C) and finally MoVTeNb-M1 (reduction temperature 520 °C). In fact, a Mars–van Krevelen mechanism is assumed for these types of catalysts, where lattice oxygen participating in the reaction is replenished by molecular oxygen species. In conclusion, based on our study, the controlling step dictating the selectivity to ethylene

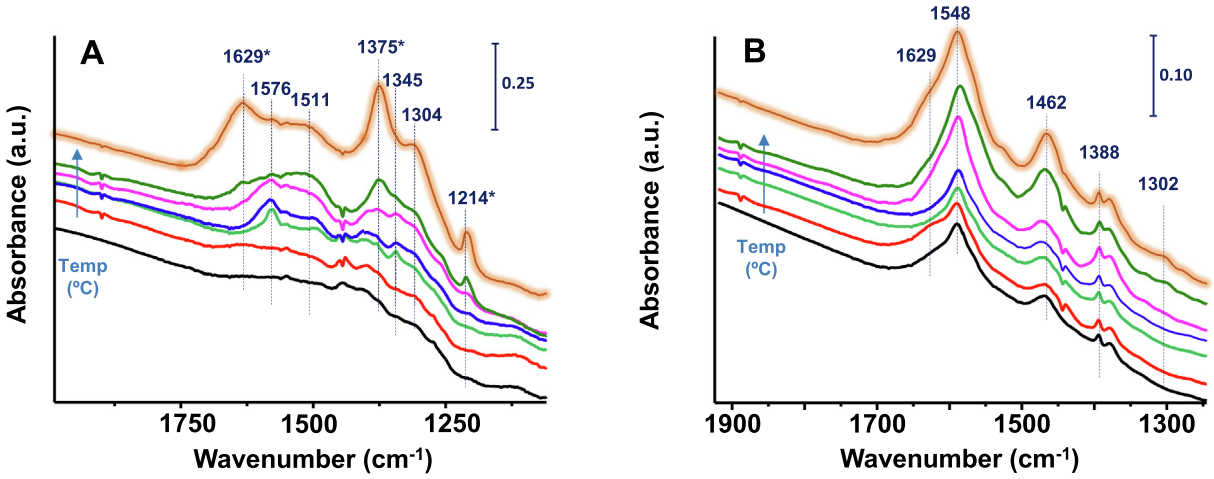

Fig. 9. IR spectra of the coadsorption of 43 mbar ethylene and 84 mbar O_2 on NiSnOx (A) or VOx/Al_2O_3 (B) at increasing reaction temperatures at constant reaction pressure (~128 mbar): 25 °C (red); 100 °C (green); 150 °C (blue); 200 °C (magenta); 250 °C light gray (dark green). Cooling to 25 °C (highlighted orange line). In black, reference spectrum prior to ethylene adsorption. In asterisks, bands due to readsorption of ethylene. (For interpretation of the references to colour in this figure legend, the reader is referred to the web version of this article.)

can be ascribed to the reactivity of surface oxygen species in each catalyst.

4. General remarks

To explain the catalytic behavior of the studied catalysts, it would be necessary to consider not only the crystalline structure of the material but also the nature and characteristics of the active centers and the influence of the environments of these active centers on the selectivity of the studied reactions. Thus, the reducibility of the active centers, the reactivity of oxygen species on the catalyst surfaces, and the adsorption/desorption capacity of reactants and products on the catalyst surfaces are key aspects for defining the catalytic behavior of a catalyst [1–9].

It is generally accepted that the selectivity to the main reaction products during the ethane ODH can be explained by considering a simplified reaction network, with parallel and consecutive reactions (Schemes 1a and 1b, in which k_1, k_2, and k_3 are kinetic constants) [13–18]. The initial selectivity to ethylene (at low conversion of alkane) is related to the k_1/k_2 ratio, while the selectivity to ethylene at high ethane conversion can be related to the $k_1/(k_2 + k_3)$ ratio. According to the catalytic results during ethane and ethylene oxidation (Fig. 4–6), important differences among catalysts can be concluded to exist (i) in the nature of deep oxidation products and (ii) in the k_2/k_1 ratio for catalysts.

One important difference between NiO-based catalysts and V-containing catalysts is related to the nature of deep oxidation products during ethane or ethylene oxidation (Fig. 5): CO_2 for NiO-containing catalysts and CO/CO_2 for V-containing catalysts. This behavior can be explained by considering the catalytic performance of these catalysts during oxidation of CO (Fig. 7). But, in addition, the results of Fig. 7 suggest that the capability of a catalyst for CO oxidation is not a key factor in developing selective catalysts for ethane ODH. In fact, unpromoted-NiO and promoted-NiO catalysts are both very effective in CO oxidation [24–30], whereas their catalytic performances in ethane ODH are completely different. In the case of V-containing catalysts, strong differences in the selectivity to ethylene from ethane depending on the support, vanadia content, and preparation method have been reported, presenting both CO and CO_2 as deep oxidation products in all cases [17–21,33–40]. Therefore, there is not a clear parallelism between the CO/CO_2 ratio and the selectivity to ethylene during ethane ODH.

Thus, a classification of catalysts for C_3–C_4 olefin oxidation according to the type of metal–oxygen bond and their behavior for CO oxidation was proposed [63]. However, this classification cannot be completely considered for either ethylene oxidation or ethane ODH.

On the other hand, the three catalysts present strong differences in the rate of transformation of ethane and ethylene (i.e., r_{C2H4}/r_{C2H6} ratios in Fig. 6), which explain the differences in selectivity to ethylene at high ethane conversions, during its ODH of ethane, and which would determine the strong dissimilarities in the k_2/k_3 ratios in Scheme 1. These variations among catalysts are probably due to significant differences in their physico–chemical properties.

Regarding the nature of these catalysts (promoted and/or supported materials), V-sites or Ni-sites can be proposed as the active sites for ethane ODH. In each case the presence of dopant and/or support strongly modifies the performance of the corresponding pure metal oxide, NiO [26–30], V_2O_5 [16,17], or MoO_3 [14,16,17]. This is due to the modification of active sites providing lattice oxygen species for hydrogen abstraction from ethane [19,21,26,28,44,47], which leads to the presence of a higher/lower concentration of nucleophilic oxygen species, depending on the catalytic system.

In the case of the Sn-doped NiO catalyst, the presence of the dopant modifies the nature of the active centers (as shown by XPS) by increasing the concentration of nucleophilic oxygen species (according to the $^{18}O_2$ isotopic exchange results [28]), in the same way as those proposed in NiO catalysts doped with niobium [26,27].

In the case of the VOx/Al_2O_3 catalyst, the support modifies the characteristics of the active sites, favoring the presence of tetragonal VO_4 species less reactive than the vanadium species in V_2O_5 [18–22], and also favoring changes in the nature of the oxygen species [64]. However, the high concentration of V^{5+} species (determined by XPS) favors the activation of both ethane and ethylene on the same active centers [18–21], resulting in a lower selectivity to ethylene at high ethane conversions. In this sense, it has been observed that an initial decrease in V^{5+} species (by treatment with H_2) favors an increase in ethylene selectivity [21]. In this way, it has recently been proposed that Al_2O_3-supported W–V–O bronze catalysts [66], presenting isolated octahedral V-species, but with higher V^{4+}/V^{5+} concentrations than those observed for conventional supported vanadium oxide catalysts, seem to be among

the most active and selective catalysts for ethane ODH on supported vanadium oxide catalysts.

In the case of the MoVTeNb-M1 catalyst, its crystalline structure corresponds to an orthorhombic bronze of Mo (the so-called M1). In catalytic terms, this catalyst can be considered as a monolayer with active centers on the catalyst surface (in the ab plane), which are not strictly a part of the M1 crystal structure [67]. In other words, the M1 phase would be the support that enables the formation of a thin active surface layer that contains $Mo^{6+}/Mo^{5+}/V^{4+}/V^{5+}$ in close vicinity to Te^{4+} oxo-sites and pentagonal Nb^{5+}-containing units [67]. In addition, the presence of Nb atoms in optimized catalysts [33–44] has been related to the elimination of Brønsted sites after the incorporation of Nb^{5+} into the framework of the catalyst [41].

In this sense, it has been observed that during the ethane ODH, MoVTeNbO catalysts are more selective to ethylene at high ethane conversions than MoVTeO [47], which seems to be more effective than Mo–V–O [40] catalysts. The concentrations of nucleophilic oxygen species in MoVTeNbO-based catalysts are higher than those in Nb-free MoVTeO catalysts [47]. Therefore, in some way, we can describe MoVTeNb-M1 catalysts as surfaces of Mo–V–Te–Nb–O mixed metal oxides on the crystalline M1 phase, in which the reaction conditions could modify the nature of the surface species, especially V-sites [37,67].

Accordingly, the presence of a promoter (in Sn-doped NiO catalyst), a support (in alumina-supported vanadium oxide catalyst), or both (in the case of MoVTeNb-M1 catalyst) exerts a positive role in selectivity to ethylene during ODH of ethane by modifying the reducibility of the active centers and the nature of the surface oxygen species (favoring an increase in nucleophilic species with respect to pure metal oxides). However, there is an additional aspect of the MoVTeNbO-M1 catalyst that is not seen in the other catalysts. This catalyst contains heptagonal channels (a seven-membered channel is a micropore with a diameter of ca. 0.4 nm) in which gases smaller than or equal to ethane can enter [36]. In fact, and especially for Mo–V–O materials with structure M1 [36,68,69], they have the ability to incorporate ethane and/or ethylene inside the heptagonal channels of the M1 phase.

Thus, the existence of microporosity in the M1 phase [68,69] could explain the results of microcalorimetry (achieved at low temperature and high partial pressures of hydrocarbon), in which an adsorption energy for the MoVTeNb-M1 higher than those for the other two catalysts is observed.

Nevertheless, it seems unlikely that this confining effect of ethane or ethylene in the pores of the catalyst is carried out at temperatures of 350–400 °C (temperatures used in the oxidation reactions of ethane and ethylene), especially considering the molecules along the micropores. In fact, the catalytic results suggest that the activity and selectivity to ethylene during the ODH of ethane are more related to the activation of ethane at the entrance of the pores rather than along the micropores.

In this way, the infrared results of CO or ethylene at low temperature (Figs. 2 and 3) suggest a greater and stronger adsorption in the case of the MoVTeNb-M1 catalyst, which could be explained by confinement of the molecules within the heptagonal channels. This does not occur in the other two catalysts.

On the other hand, the IR spectroscopy results of adsorbed ethylene and the evolution with temperature of the adsorbed species suggest that, in the case of the MoVTeNb-M1 catalyst (Fig. 8), there is low catalytic activity for the oxidation of ethylene, which is in agreement with the ODHE catalytic results (Fig. 6a). This behavior is completely different from previous results on the IR spectroscopy of adsorbed propylene on a similar MoVTeNbO catalyst, in which a high reactivity of propylene (with the formation of π-allylic intermediate) and the formation of partial oxidation products (mainly acrylic acid) were observed [60]. The different natures of the two olefins (especially the presence of allylic hydrogen in propylene) strongly influence their reactivity on multicomponent MoVTeNbO catalysts, changing the nature and reactivity of adsorbed species during the adsorption of ethylene or propylene.

Conversely, in the case of NiSnOx and VOx/Al_2O_3 catalysts, the results of adsorbed ethylene spectroscopy suggest relatively high catalytic activity for the oxidation of ethylene, especially for the latter, which is in agreement with the catalytic results (Fig. 6b and 6c, respectively). This behavior is similar to that achieved by IR spectroscopy of propylene over supported vanadium oxide catalysts [60].

A relationship between adsorption and reactivity is difficult to establish, provided that additional parameters, such as the reactivity of surface oxygen species, play an important role in olefin overoxidation and accordingly decreases the selectivity in the ODH reaction. In situ IR studies (Figs. 8 and 9) and TPR H_2 data (Fig. 1) showed an intimate correlation between catalyst reducibility (Me−O bond strength) and ethylene overoxidation in the IR work. In this case, fast overoxidation is observed in the NiSnOx sample, exhibiting the lowest reduction temperature in the TPR pattern (320 °C), followed by the VOx/Al_2O_3 sample (475 °C), while no overoxidation is observed in MoVTeNb-M1, which is the catalyst that presented the highest reduction temperature (500 °C). Analyzing the catalytic data, a drastic decrease in the selectivity to ethylene is observed on VOx/Al_2O_3 catalyst compared with NiSnOx, when the ethane conversion increases, while practically constant selectivity is observed on the MoVTeNb-M1 sample. Notoriously, based on IR data, while a higher overoxidation ability is observed on the NiSnOx sample versus VOx/Al_2O_3, uncovered surface sites are observed on the NiSnOx sample, as determined in the cooling-down experiments, favoring the selective dehydrogenation path, and resulting in a lower extension of ethylene deep oxidation compared with that observed on the VOx/Al_2O_3 catalyst.

The number and nature of active sites determined from adsorption calorimetry measurements for the different catalysts can help us to understand their different catalytic behavior. If the adsorption is too strong or too weak, the reactivity is usually low [70]. Strong adsorptions prevent the replacement of reactant molecules on the catalyst surface, covering potential active sites and then avoiding high reactivity. Likewise, weak adsorptions mean that just a portion of the catalyst surface is covered by the reactant and thus the reactivity is low. The heat of ethane adsorption on MoVTeNb-M1 (32 kJ mol^{-1}) is in good agreement with that previously reported [37], which is not too high but allows good reactant–surface interaction. However, the strength of adsorption of ethane on NiSnOx or VOx/Al_2O_3 surface is very low (10–13 kJ mol^{-1}, which are values very close to the heat of condensation of the ethane molecule [37]), suggesting that there is not a strong interaction between the molecules and the surfaces of these catalysts. Thus, the results from microcalorimetry indicate that M1-containing catalysts have active sites more appropriate for ethane activation than VOx/Al_2O_3 and NiSnOx catalysts. Moreover, despite the lower specific surface area of MoVTeNb-M1, this catalyst is more active per active site and, most importantly, more selective to ethylene in the ethane ODH than VOx/Al_2O_3 and NiSnOx. The density of surface active sites for ethane adsorption is much higher for MoVTeNb-M1 than for VOx/Al_2O_3 and NiSnOx. In addition, the adsorption enthalpy of ethylene on MoVTeNb-M1 catalyst is slightly higher with respect to ethane. One can expect that the high selectivity of this catalyst is related to the high capability for the abstraction of H from the C–H bond in ethane by breaking it, and a lower reactivity in the oxidation of the resulting ethylene. For MoVTeNb-M1 catalyst, the ethane reaction can stop at the formation of ethylene, favored by the slightly higher adsorption heat of ethylene on MoVTeNb-M1 catalyst (Table 2). In this situation, high surface coverage by ethane and ethylene molecules can make simultaneous O_2 chemisorption difficult.

The characteristics of the active sites in the MoVTeNb-M1 catalyst lead to selective ethane activation by H-abstraction and could avoid O-insertion, thus preventing further oxidation, and resulting in higher selectivity to the olefin in the ODH process.

If the activity per active site and per surface area is considered, even larger differences between MoVTeNb-M1 (6.8 $mmol_{C2H6}\ m^{-2}h^{-1}$) and VOx/Al_2O_3 and NiSnOx (0.09 and 0.31 $mmol_{C2H6}\ m^{-2}h^{-1}$, respectively) can be observed. V-sites in the M1 environment are ca. 70 times more reactive than V-sites supported on alumina, whereas the amount of V-species on the corresponding catalyst surface is similar. The presence of Te-free heptagonal channels [72,73], since at the entrance of the heptagonal channels the hydrogen abstraction would be produced, and the higher adsorption energy could explain this remarkable difference in reactivity.

The rate-determining step in the ODH of ethane on redox metal oxide catalysts is the C–H activation, which requires partial reduction of the metal site [13–17]. After the C–H activation, an alkyl radical intermediate is formed that, depending on the environment, will lead to a second H-removal to form the desired olefin or to O-insertion to form carbon oxides [13–17,71,72]. Similarly, the olefin formed also could evolve to alkyl radicals, which in this case only would have oxygen insertion. However, the results presented here clearly indicate that the behavior in ethane and ethylene oxidation is different in the catalysts tested. The multicomponent Mo–V–Te–Nb mixed oxides catalyst is the one with the highest initial selectivity to the olefin and the lowest ethylene overoxidation, whereas the supported VOx/Al_2O_3 catalyst is the one with the lowest initial ethylene formation and the highest ethylene combustion. The MoVTeNb-M1 catalyst tends to a second C–H activation from ethane once the alkyl radical is formed. Also, the ethylene molecule formed is kept without reacting. On the other hand, supported VOx/Al_2O_3 catalyst, once the ethylene molecule is formed, undergoes to carbon oxides formation by O-insertion in the intermediate alkyl radical. As mentioned above, the different highest yields that can be achieved with these catalysts are related to the different relative reactivities of ethane and ethylene (drop of ethylene selectivity). Thus, in the M1 catalyst, the active sites are much more reactive for ethane than for ethylene activation (reactivity ethylene/ethane ratio of 0.072). Something similar but less marked happens with the NiSnOx catalyst (reactivity ethylene/ethane ratio of 0.21). However, with the VOx/Al_2O_3 catalyst, ethylene oxidation takes place with a reaction rate 2.6 times higher that of ethane oxidation. The relationship between adsorption and selectivity to a given product is not easy, but strong chemisorption of the desired compound on the surface of the catalyst often leads to its decomposition and consequently to a fall of selectivity to the desired compound. Thus, stronger adsorption of the olefin formed could favor its decomposition, but it does not take place on the MoVTeNb-M1 sample. In fact, the heat of ethylene adsorption on MoVTeNb-M1 catalyst at low temperature is higher than that of ethane, whereas the deep oxidation of the olefin at 300–400 °C is still extremely low. However, V-sites in the M1 environment present an extremely low ability to activate ethylene in spite of rather strong adsorption. A low concentration of oxygen and an extremely low stability of O-insertion intermediates due to steric hindrance in the micropores [36,39,68,69], or in the window of the heptagonal channels [72,73], has been proposed as the reason for this high olefin selectivity.

5. Conclusions

The different catalytic performance of the three most significant catalysts reported during the past decades for the oxidative dehydrogenation of ethane to ethylene (MoVTeNbO mixed metal oxides, Sn-doped NiO, and Al_2O_3-supported vanadium oxide) has been studied comparatively. The main difference in catalytic performance in ethane ODH over these catalysts cannot be related only to a variable extent of ethylene oxidation but also to the strong differences between ethane and ethene oxidation over these catalysts. The overoxidation of ethylene is the highest for the VOx/Al_2O_3 catalyst and the lowest for MoVTeNb-M1, with NiSnOx catalyst presenting intermediate behavior. In addition, when the reaction rates for ethane and ethylene oxidation are considered, a reactivity for ethane oxidation more than 10 times higher than that for ethylene oxidation (the r_{C2H4}/r_{C2H6} ratio is 0.073 at 400 °C) is observed over the MoVTeNb-M1 catalyst, in contrast with r_{C2H4}/r_{C2H6} ratios of 0.21 (NiSnOx) and 2.58 (VOx/Al_2O_3) under the same reaction conditions. These results are in agreement with the high selectivity to ethylene achieved over MoVTeNb-M1 catalyst (with yield of ethylene of ca. 75%), with a large drop in the selectivity to ethylene observed over VOx/Al_2O_3 catalyst during ethane ODH when the ethane conversion increases (and yield of ethylene up to 6%), and intermediate behavior observed for NiSnOx catalysts (with yield of ethylene up to 30%).

To understand these catalytic behaviors better, microcalorimetry of adsorption of ethane or ethylene, infrared study of adsorbed species (CO, NH_3 and ethylene) at low temperature, and in situ IR study of ethylene and O_2 coadsorption (under reaction conditions) were carried out. Both the microcalorimetry results and the infrared study at low temperature for adsorbed ethylene suggest that MoVTeNb-M1 shows the highest heat of adsorption for both ethane and ethylene (with ethylene interacting slightly more strongly than ethane) on the surface of this catalyst and higher interaction strength between ethylene and Lewis acid sites. However, VOx/Al_2O_3 and NiSnOx catalysts present a very low interaction with ethane or ethylene at low temperature.

The different catalytic behavior of these catalysts can be better explained from a comparison of ethylene oxidation results and in situ IR studies of ethylene and O_2 co-adsorption experiments. A fast desorption of ethylene is observed at 100 °C over MoVTeNb-M1 catalysts (without any additional IR signal), suggesting the nonexistence of a reaction between ethylene and oxygen. In an opposite trend, NiSnOx and VOx/Al_2O_3 catalysts present several IR bands during ethylene/O_2 coadsorption experiments (moderate temperatures) indicating the appearance of O-containing compounds, which can be transformed into carbon oxides at higher temperatures. Accordingly, the high stability of ethylene on MoVTeNb-M1 active sites is not due to weak adsorption of ethylene but to the limited ability of its active sites to activate ethylene. Although the results presented here suggest that the presence of V^{4+} species (a majority in MoVTeNb-M1 and a minority in VOx/Al_2O_3) improves selectivity to ethylene, it does not seem to be sufficient to explain the catalytic behavior of catalysts presenting the M1 phase. In fact, the results obtained for a supported vanadium-containing hexagonal tungsten bronze ($W–V–O/Al_2O_3$ catalyst [66]), which mostly presents V^{4+} species, show catalytic behavior in ethane ODH better than that of VOx/Al_2O_3 but worse than that of MoVTeNb-M1. Thus, the catalytic performance of Mo–V–Te–Nb–O mixed oxides can be related to the presence of heptagonal channels in the M1 structure (with size similar to the kinetic diameter of ethane/ethylene molecules, ca. 4.0 Å), in whose entrance the H-abstraction of ethane could be carried out, in agreement with other authors [33–40,67–69]. The low specificity of isolated V^{4+} species to ethylene transformation (probably in V–O–Mo pairs inside the heptagonal channels) can be a key factor in the high selectivity to ethylene.

Declaration of Competing Interest

The authors declare that they have no known competing financial interests or personal relationships that could have appeared to influence the work reported in this paper.

Acknowledgments

The authors acknowledge the Spanish Ministry of Science, Innovation and Universities (MCIU) for their funding (RTI2018-099668-B-C21, MAT2017-84118-C2-1-R and MAT2017-87500-P) and FEDER. The authors from ITQ also thank Programa Severo Ochoa (SEV-2016-0683). A.A. acknowledges the Severo Ochoa Excellence Program for his grant (BES-2017-080329).

Appendix A. Supplementary material

Supplementary data to this article can be found online at https://doi.org/10.1016/j.jcat.2021.07.015.

References

[1] J. Haber, Oxidation of hydrocarbons, in: G. Ertl, H. Knoezinger, J. Weitkamp (Eds.), Handbook of Heterogeneous Catalysis, vol. 4.6.2., Wiley-VCH, 1997, pp. 2253–2274.
[2] R.K. Grasselli, Ammoxidation, in: G. Ertl, H. Knoezinger, J. Weitkamp (Eds.), Handbook of Heterogeneous Catalysis, vol. 4.6.6, Wiley-VCH, 1997, pp. 302 (and references therein).
[3] J. Haber, The concept of structure-sensitivity in catalysis by oxides, Stud. Surf. Sci. Catal. 48 (1989) 447–466.
[4] J. Haber, Catalytic oxidation- State of the art and prospects, Stud. Surf. Sci. Catal. 72 (1992) 279–304.
[5] J. Haber, Selectivity in Heterogeneous Catalytic Oxidation of Hydrocarbons, in Heterogeneous Hydrocarbon Oxidation, ACS Symp. Series 638 (1996) 20–34.
[6] R.K. Grasselli, Site isolation and phase cooperation: Two important concepts in selective oxidation catalysis: A retrospective, Catal. Today 238 (2014) 10–27.
[7] R.K. Grasselli, J.D. Burrington, D.J. Buttrey, P. DeSanto Jr., Cl.G. Lugmair, A.F. Volpe Jr., T. Weingand, Multifunctionality of active centers in (amm)oxidation catalysts: from Bi–Mo–Ox to Mo–V–Nb–(Te;Sb)–Ox, Top. Catal. 23 (2003) 5–22.
[8] R.K. Grasselli, Fundamental principles of selective heterogeneous oxidation catalysis, Top. Catal. 21 (2002) 79–88.
[9] Robert K. Grasselli, Advances and future trends in selective oxidation and ammoxidation catalysis, Catal. Today 49 (1999) 141–153.
[10] E.G. Rightor, C.L. Tway, Global energy & emissions reduction potential of chemical process improvements, Catal. Today 258 (2015) 226–229.
[11] Chinmoy Baroi, Anne M. Gaffney, Rebecca Fushimi, Process economics and safety considerations for the oxidative dehydrogenation of ethane using the M1 catalyst, Catal. Today 298 (2017) 138–144.
[12] Anne M. Gaffney, Jacob W. Sims, Vincent J. Martin, Natalie V. Duprez, Kelsey J. Louthan, Kenneth L. Roberts, Evaluation and analysis of ethylene production using oxidative dehydrogenation, Catal. Today 369 (2021) 203–209.
[13] F. Cavani, N. Ballarini, A. Cericola, Oxidative dehydrogenation of ethane and propane: How far from commercial implementation?, Catal Today 127 (2007) 113–131.
[14] C.A. Gärtner, A.C. van Veen, J.A. Lercher, Oxidative Dehydrogenation of Ethane: Common Principles and Mechanistic Aspects, ChemCatChem 5 (2013) 3196–3217.
[15] Joseph T. Grant, Juan M. Venegas, William P. McDermott, Ive Hermans, Aerobic Oxidations of Light Alkanes over Solid Metal Oxide Catalysts, Chem. Rev. 118 (5) (2018) 2769–2815.
[16] José M. López Nieto, The Selective Oxidative Activation of light Alkanes. From Supported Vanadia to Multicomponent Bulk V-Containing Catalysts, Top. Catal. 41 (1-4) (2006) 3–15.
[17] H.H. Kung, Oxidative dehydrogenation of light (C_2 to C_4) alkanes, Adv. Catal. 40 (1994) 1–38.
[18] T. Blasco, A. Galli, J.M. López Nieto, F. Trifiró, Oxidative Dehydrogenation of Ethane and n-Butane on VOx/Al_2O_3 Catalysts, J. Catal. 169 (1) (1997) 203–211.
[19] K. Chen, A.T. Bell, E. Iglesia, The Relationship between the Electronic and Redox Properties of Dispersed Metal Oxides and Their Turnover Rates in Oxidative Dehydrogenation Reactions, J. Catal. 209 (2002) 35–42.
[20] Morris D. Argyle, Kaidong Chen, Alexis T. Bell, Enrique Iglesia, Effect of Catalyst Structure on Oxidative Dehydrogenation of Ethane and Propane on Alumina-Supported Vanadia, J. Catal. 208 (2002) 139–149.
[21] Arne Dinse, Reinhard Schomäcker, Alexis T. Bell, The role of lattice oxygen in the oxidative dehydrogenation of ethane on alumina-supported vanadium oxide, Phys. Chem. Chem. Phys. 11 (2009) 6119, https://doi.org/10.1039/b821131k.
[22] Benjamin Frank, Rémy Fortrie, Christian Hess, Robert Schlögl, Reinhard Schomäcker, Reoxidation dynamics of highly dispersed VOx species supported on γ-alumina, Appl. Catal. A Gen 353 (2) (2009) 288–295.
[23] Hacksung Kim, Glen A. Ferguson, Lei Cheng, Stan A. Zygmunt, Peter C. Stair, Larry A. Curtiss, Structure-Specific Reactivity of Alumina-Supported Monomeric Vanadium Oxide Species, J. Phys. Chem. C 116 (4) (2012) 2927–2932.
[24] a) E. Heracleous, A.A. Lemonidou, Ni–Nb–O mixed oxides as highly active and selective catalysts for ethene production via ethane oxidative dehydrogenation. Part I: Characterization and catalytic performance, J. Catal. 237 (2006) 162–174;
b) E. Heracleous, A.A. Lemonidou, Ni–Nb–O mixed oxides as highly active and selective catalysts for ethene production via ethane oxidative dehydrogenation. Part II: Mechanistics aspects and kineting modeling, J. Catal. 237 (2006) 175–189.
[25] (a) Liu, US Patent 6, 891,075, 2005;
(b) Y. Liu, U.S. Patent 7,227,049 A2, 2007 (Assigned to Symyx Solutions Inc).
[26] E. Heracleous, A.F. Lee, K. Wilson, A.A. Lemonidou, Investigation of Ni-based alumina-supported catalysts for the oxidative dehydrogenation of ethane to ethylene: structural characterization and reactivity studies, J. Catal. 231 (2005) 159–171.
[27] E. Heracleous, A.A. Lemonidou, Ni–Me–O mixed metal oxides for the effective oxidative dehydrogenation of ethane to ethylene- Effect of promoting metal Me, J. Catal. 270 (2010) 67–75.
[28] B. Solsona, P. Concepción, B. Demicol, S. Hernández, J.J. Delgado, J.J. Calvino, J. M. López Nieto, Selective oxidative dehydrogenation of ethane over SnO_2-promoted NiO catalysts, J. Catal. 295 (2012) 104–114.
[29] H. Zhu, D.C. Rosenfeld, M. Harb, D.H. Anjum, M.N. Hedhili, S. Ould-Chikh, J.M. Basset, Ni−M−O (M = Sn, Ti, W) Catalysts Prepared by a Dry Mixing Method for Oxidative Dehydrogenation of Ethane, ACS Catal. 6 (2016) 2852–2866.
[30] J.M. López Nieto, B. Solsona, R.K. Grasselli, P. Concepcion, Promoted NiO Catalysts for the Oxidative Dehydrogenation of Ethane, Top. Catal. 57 (2014) 1248–1255.
[31] J.J. Varghese, S.H. Mushrif, Insights into the C−H Bond Activation on NiO Surfaces: The Role of Nickel and Oxygen Vacancies and of Low Valent Dopants on the Reactivity and Energetics, J. Phys. Chem. C 121 (2017) 17969–17981.
[32] X. Lin, Y. Xi, J. Sun, Unraveling the Reaction Mechanism for Nickel-Catalyzed Oxidative Dehydrogenation of Ethane by DFT: The C−H Bond Activation Step and its Following Pathways, J. Phys. Chem. C 116 (2012) 3503–3516.
[33] P. Botella, E. García-González, A. Dejoz, J.M. López Nieto, M.I. Vázquez, J. González-Calbet, Selective oxidative dehydrogenation of ethane on MoVTeNbO mixed metal oxide catalysts, J. Catal. 225 (2004) 428–438.
[34] J.M. López Nieto, P. Botella, M.I. Vázquez, A. Dejoz, U.S. Patent 7,319,179 B2, 2008 (Assigned to CSIC and UPV).
[35] P. Botella, A. Dejoz, M.C. Abelló, M.I. Vázquez, L. Arrúa, J.M. López Nieto, Selective oxidation of ethane. Developing an orthorhombic phase in Mo-V-X (X=Nb, Sb, Te) mixed oxides, Catal. Today 142 (2009) 272–277.
[36] a) T. Konya, T. Katou, T. Murayama, S. Ishikawa, M. Sadakane, D. Buttrey, W. Ueda, An orthorhombic Mo_3VO_x catalyst most active for oxidative dehydrogenation of ethane among related complex metal oxides, Catal. Sci. Technol. 3 (2013) 380–387;
b) S. Ishikawa, D. Kobayashi, T. Konya, S. Ohmura, T. Murayama, N. Yasuda, M. Sadakane, W. Ueda, Redox Treatment of Orthorhombic $Mo_{29}V_{11}O_{112}$ and Relationships between Crystal Structure, Microporosity and Catalytic Performance for Selective Oxidation of Ethane, J. Phys. Chem. C 119 (2015) 7195–7206.
[37] P. Kube, B. Frank, S. Wrabetz, J. Kröhnert, M. Hävecker, J. Velasco-Vélez, J. Noack, R. Schlögl, A. Trunschke, Functional Analysis of Catalysts for Lower Alkane Oxidation, ChemCatChem 9 (2017) 573–585.
[38] P.J. Donaubauer, D.M. Melzer, K. Wanninger, G. Mestl, M. Sanchez-Sanchez, J.A. Lercher, O. Hinrichsen, Intrinsic kinetic model for oxidative dehydrogenation of ethane over MoVTeNb mixed metal oxides: A mechanistic approach, Chem. Eng. J. 383 (2020) 123195.
[39] L. Annamalai, Y. Liu, S. Ezenwa, Y. Dang, S.L. Suib, P. Deshlahra, Influence of Tight Confinement on Selective Oxidative Dehydrogenation of Ethane on MoVTeNb Mixed Oxides, ACS Catal. 8 (2018) 7051–7067.
[40] a) D. Melzer, G. Mestl, K. Wanninger, Y. Zhu, N.D. Browning, M. Sanchez-Sanchez, J.A. Lercher, Design and synthesis of highly active MoVTeNb oxides for ethane oxidative dehydrogenation, Nat. Commun. 10 (2019) 4012;
b) D. Melzer, P. Xu, D. Hartmann, Y. Zhu, N.D. Browning, M. Sanchez-Sanchez, J.A. Lercher, Atomic-Scale Determination of Active Facets on the MoVTeNb Oxide M1 Phase and Their Intrinsic Catalytic Activity for Ethane Oxidative Dehydrogenation, Angew. Chem. Int. Ed. 55 (2016) 8873–8877.
[41] M. Baca, A. Pigamo, J.L. Dubois, J.M.M. Millet, Catal. Commun. 6 (2005) 215–220.
[42] S. Lwin, W. Diao, Ch.y. Baroi, A.M. Gaffney, R.R. Fushimi, Characterization of MoVTeNbOx Catalysts during Oxidation Reactions Using In Situ/Operando Techniques, A Review, Catalysts 7 (2017) 109.
[43] A.M. Gaffney, Q. An, W.A. Goddard III, W. Diao, M.V. Glazoff, Toward Concurrent Engineering of the M1-Based Catalytic Systems for Oxidative Dehydrogenation (ODH) of Alkanes, Top. Catal. 63 (2020) 1667–1681.
[44] J.M. López Nieto, P. Botella, P. Concepción, A. Dejoz, M.I. Vázquez, Oxidative dehydrogenation of ethane on Te-containing MoVNbO catalysts, Catal. Today 91–92 (2004) 241–245.
[45] G.C. Bond, K. Bruckman, Selective oxidation of o-xylene by monolayer V_2O_5-TiO_2 catalysts, Faraday Discuss. Chem. Soc. 72 (1981) 235–246.
[46] X. Wang, B. Zhao, D. Jiang, Y. Xie, Monolayer dispersion of MoO_3, NiO and their precursors on γ-Al_2O_3, Appl. Catal. A Gen. 188 (1999) 201–209.
[47] P. Concepcion, S. Hernandez, J.M. Lopez Nieto, On the nature of active sites in MoVTeO and MoVTeNbO catalysts: The influence of catalyst activation temperature, Appl. Catal. A Gen. 391 (2011) 92–101.
[48] L. Koudelka, J. Pospísil, P. Mosner, L. Montagne, L. Delevoye, Structure and properties of potassium niobato-borophosphate glasses, J. Non-Cryst. Solids 354 (2008) 129–133.

[49] D. Delgado, B. Solsona, R. Sanchis, E. Rodriguez-Castellón, J.M. López Nieto, Oxidative dehydrogenation of ethane on diluted or promoted nickel oxide catalysts: Influence of the promoter/diluter, Catal. Today 363 (2021) 27–35.
[50] E. Aytan, B. Debnath, F. Kargar, Y. Barlas, M.M. Lacerda, J.X. Li, R.K. Lake, J. Shi, A.A. Balandin, Spin-phonon coupling in antiferromagnetic nickel oxide, Appl. Phys. Lett. 111 (2017) 252402.
[51] a) M.A. Vuurmant, I.E. Wachs, In Situ Raman Spectroscopy of Alumina-Supported Metal Oxide Catalysts, J. Phys. Chem. 96 (1992) 5008–5016;
b) Z. Wu, H.-S. Kim, P.C. Stair, S. Rugmini, S.D. Jackson, On the Structure of Vanadium Oxide Supported on Aluminas: UV and Visible Raman Spectroscopy, UV-Visible Diffuse Reflectance Spectroscopy, and Temperature-Programmed Reduction Studies, J. Phys. Chem. B 109 (2005) 2793–2800.
[52] L.E. Briand, O.P. Tkachenko, M. Guraya, X. Gao, I.E. Wachs, W. Grünert, Surface-Analytical Studies of Supported Vanadium Oxide Monolayer Catalysts, J. Phys. Chem. B 108 (2004) 4823–4830.
[53] A. Massó Ramirez, F. Ivars-Barceló, J.M. López Nieto, Optimizing Reflux Synthesis Method of Mo-V-Te-Nb mixed oxide Catalysts for Light Alkane Selective Oxidation, Catal. Today 356 (2020) 322–329.
[54] D. Delgado, B. Solsona, A. Ykrelef, A. Rodríguez-Gómez, A. Caballero, E. Rodríguez-Aguado, E. Rodríguez-Castellón, J.M. López Nieto, Redox and Catalytic Properties of Promoted NiO Catalysts for the Oxidative Dehydrogenation of Ethane, J. Phys. Chem. C 121 (2017) 25132–25142.
[55] J.M. López Nieto, J. Soler, P. Concepcion, J. Herguido, M. Menendez, J. Santamaria, Oxidative Dehydrogenation of Alkanes over V-based Catalysts: Influence of Redox Properties on Catalytic Performance, J. Catal. 185 (1999) 324–332.
[56] a) P. Concepción, K. Hajiivanov, H. Knözinger, Low-Temperature CO Adsorption on V-Containing Aluminophosphates: An FTIR Study, J. Catal. 184 (1999) 172–179;
b) K.I. Hadjiivanov, G.N. Vayssilov, Characterization of oxides surfaces and zeolites by carbon monoxide as IR probe molecule, Adv. Catal. 47 (2002) 307–511.
[57] G. Busca, V. Lorenzelli, V. Sánchez-Escribano, Preparation, solid-state characterization, and surface chemistry of high-surface-area nickel-aluminum ($Ni_xAl_{2-2x}O_{3-2x}$) mixed oxides, Chem. Mater. 4 (1992) 595–605.
[58] N. Sergent, P. Gelin, L. Perier-Camby, H. Praliaud, G. Thomas, FTIR study of low-temperature CO adsorption on high surface area tin(IV) oxide: Probing Lewis and Brønsted acidity, Phys. Chem. Chem. Phys. 4 (2002) 4802–4808.
[59] J.M. Gallardo Amores, V. Sanchez Escribano, G. Ramis, G. Busca, An FT-IR study of ammonia adsorption and oxidation over anatase-supported metal oxides, Appl. Catal. B Environ. 13 (1997) 45–58.
[60] P. Concepción, P. Botella, J.M. López Nieto, Catalytic and FT-IR study on the reaction pathway for oxidation of propane and propylene on V- or Mo–V-based catalysts, Appl. Catal. A Gen. 278 (2004) 45–56.
[61] a) G. Busca, V. Lorenzelli, G. Ramis, J. Saussey, J.C. Lavalley, FT-IR spectra of ethylene molecularly adsorbed on metal oxides, J. Mol. Struct. 267 (1992) 315–329;
b) V. Sanchez Escribano, G. Busca, V. Lorenzelli, Fourier Transform Infrared Spectroscopic Studies of the Reactivity of Vanadia-Titania Catalysts toward Olefins. 2. Ethylene, J. Phys. Chem. 94 (1990) 8945–8948.
[62] D. Delgado, R. Sanchis, B. Solsona, P. Concepción, J.M. López Nieto, Influence of the Nature of the Promoter in NiO Catalysts on the Selectivity to Olefin During the Oxidative Dehydrogenation of Propane and Ethane, Top. Catal. 63 (2020) 1731–2174.
[63] F. Trifiró, I. Pasquon, Classification of oxidation catalysts according to the type of metal-oxygen bond, J. Catal. 12 (1968) 412–416.
[64] C. Doornkamp, M. Clement, X. Gao, G. Deo, I.E. Wachs, V. Ponec, The Oxygen Isotopic Exchange Reaction on Vanadium Oxide Catalysts, J. Catal. 185 (1999) 415–422.
[65] K.R. William, G.E. Ewing, Infrared spectra and structure of ethane on NaCl (100), J. Phys. Chem. 99 (1995) 2186–2193.
[66] S. Benomar, A. Chieregato, A. Masso, M.D. Soriano, J.A. Vidal-Moya, T. Blasco, R. Issaadi, J.M. López Nieto, Al_2O_3-Supported W-V-O bronzes catalysts for oxidative dehydrogenation of ethane, Catal. Sci. Technol. 10 (2020) 8064–8076.
[67] M. Hävecker, S. Wrabetz, J. Kröhnert, L.-I. Csepei, R.N. d'Alnoncourt, Y.V. Kolen'ko, F. Girgsdies, R. Schlögl, A. Trunschke, Surface chemistry of phase-pure M1 MoVTeNb oxide during operation in selective oxidation of propane to acrylic acid, J. Catal. 285 (2012) 48–60.
[68] a) S. Ishikawa, X. Yi, T. Murayama, W. Ueda, Heptagonal channel micropore of orthorhombic Mo3VOx as catalysis field for the selective oxidation of ethane, Appl. Catal. A Gen 474 (2014) 10–17;
b) S. Ishikawa, W. Ueda, Microporous crystalline Mo–V mixed oxides for selective oxidations, Catal. Sci. Technol. 6 (2016) 617–629.
[69] a) M. Sadakane, K. Kodato, T. Kuranishi, Y. Nodasaka, K. Sugawara, N. Sakaguchi, T. Nagai, Y. Matsui, W. Ueda, Molybdenum-vanadium-based molecular sieves with microchannels of seven-membered rings of corner-sharing metal oxide octahedra, Angew. Chem. Int. Ed. 47 (2008) 2493–2496;
b) M. Sadakane, K. Kodato, N. Yasuda, S. Ishikawa, W. Ueda, Thermal Behavior, Crystal Structure, and Solid-State Transformation of Orthorhombic Mo−V Oxide under Nitrogen Flow or in Air, ACS Omega 4 (2019) 13165–13171.
[70] J.J. Spivey, Complete catalytic oxidation of volatile organics, Ind. Eng. Chem. Res. 26 (1987) 2165–2180.
[71] X. Rozanska, J. Sauer, Oxidative conversion of C_1–C_3 alkanes by vanadium oxide catalysts. DFT results and their accuracy, Int. J. Quantum Chem. 108 (2008) 2223–2229.
[72] J.M. López Nieto, B. Solsona, P. Concepción, F. Ivars, A. Dejoz, M.I. Vazquez, Reaction products and pathways in the selective oxidation of C_2–C_4 alkanes on MoVTeNb mixed oxide catalysts, Catal. Today 157 (2010) 291–296.
[73] P. Botella, E. García-González, J.M. López Nieto, J.M. González-Calbet, MoVTeNbO multifunctional catalysts: Correlation between constituent crystalline phases and catalytic performance, Solid State Sci. 7 (2005) 507–519.